Colder eastern equatorial Pacific and stronger Walker cell in the early 21st century: isolating the forced response to global warming

Ulla Klint Heede[1] and Alexey Fedorov[1]

[1]Yale University

November 22, 2022

Abstract

Since the early 1990s the Pacific Walker circulation shows a multi-decadal strengthening, contradicting future model projections. Whether this trend, evident in a range of indices especially before the 2015 El Niño, reflects the coupled ocean-atmosphere response to global warming or the negative phase of the Pacific Decadal Oscillation (PDO) remains debated. Here we show that sea surface temperature (SST) trends during 1980-2020 are dominated by three signals: a spatially uniform warming trend, a negative PDO pattern, and a Northern Hemisphere/Indo-West Pacific warming pattern. The latter pattern, which closely resembles the transient ocean thermostat-like response to global warming emerging in a subset of CMIP6 models, shows cooling in the central-eastern Pacific but warming in the western Pacific and tropical Indian ocean. This pattern contributes to the Walker circulation strengthening along with the PDO. Historical simulations appear to underestimate this pattern, contributing to the models' inability to replicate the Walker cell strengthening.

Colder eastern equatorial Pacific and stronger Walker cell in the early 21st century: isolating the forced response to global warming

Supplementary Material

Ulla K. Heede[1]* and Alexey V. Fedorov[1,2]

[1]Department of Earth and Planetary Science, Yale University, New Haven, CT

[2] LOCEAN/IPSL, Sorbonne University, Paris

* Corresponding author: 210 Whitney Avenue, 06511 New Haven CT, ulla.heede@yale.edu

Variable	Metric	Temporal coverage	Dataset	Source
Sea surface temperature (SST)	West (130º E to 180º E, 5º S to 5º N) minus East (160º W to 80º W, 5º S to 5º N)	1975-2021	ERSSTv5	https://psl.noaa.gov/data/gridded/data.noaa.ersst.v5.html
Sea surface height (SSH)	West (130º E to 180º E, 5º S to 5º N) minus East (160º W to 80º W, 5º S to 5º N)	1991-2021	MEaSUREs Gridded Sea Surface Height Anomalies v1812	https://podaac.jpl.nasa.gov/dataset/SEA_SURFACE_HEIGHT_ALT_GRIDS_L4_2SATS_5DAY_6THDEG_V_JPL1812

Variable	Metric	Temporal coverage	Dataset	Source
Precipitation	West (130^o E to 150^o E, 5^o S to 5^o N) minus East (180^o W to 80^o W, 5^o S to 5^o N)	1979-2021	CMAP	https://psl.noaa.gov/data/gridded/data.cmap.html
Sea level pressure (SLP)	West (130^o E to 150^o E, 5^o S to 5^o N) minus Central (160^o W to 120^o W, 5^o S to 5^o N)	1975-2021	NCEP/NCAR reanalysis	https://psl.noaa.gov/data/reanalysis/reanalysis.shtml
Outgoing longwave radiation (OLR)	Central (160^o W to 120^o W, 10^o S to 10^o N)	1979-2021	NOAA interpolated OLR	https://psl.noaa.gov/data/gridded/data.interp_OLR.html
Zonal ocean currents	Equatorial Pacific (150^o E to 80^o W, 5^o S to 5^o N)	1992-2021	OSCAR	https://podaac-tools.jpl.nasa.gov/drive/files/allData/oscar/prev/L4/oscar_third_deg/
Surface winds	Equatorial Pacific (150^o E to 80^o W, 5^o S to 5^o N)	1975-2021	NCEP/NCAR reanalysis	https://psl.noaa.gov/data/gridded/data.ncep.reanalysis.derived.surface.html
Omega (pressure velocity,ω)	West (130 ^{o} E to 150 ^{o} E, 10 ^{o} S to 10 ^{o} N)	1975-2021	NCEP/NCAR reanalysis	https://psl.noaa.gov/data/gridded/data.ncep.reanalysis.derived.surface.html

Supplementary Table 1. Overview of climatic indices used as measures of the Walker circulation strength, *including their temporal and spatial range. Indirect measures, such as the ocean surface current speed along the equator, are also included. Note that the SSH dataset we used contains only SSH anomalies, consequently to obtain SSH difference between the east and west equatorial Pacific, we first compute the time-mean SSH for each grid based on the AVISO dataset (AVISO, 2011), then we add these background SSH values to the sea-surface height anomaly (MEaSUREs Gridded Sea Surface Height Anomalies v1812).*

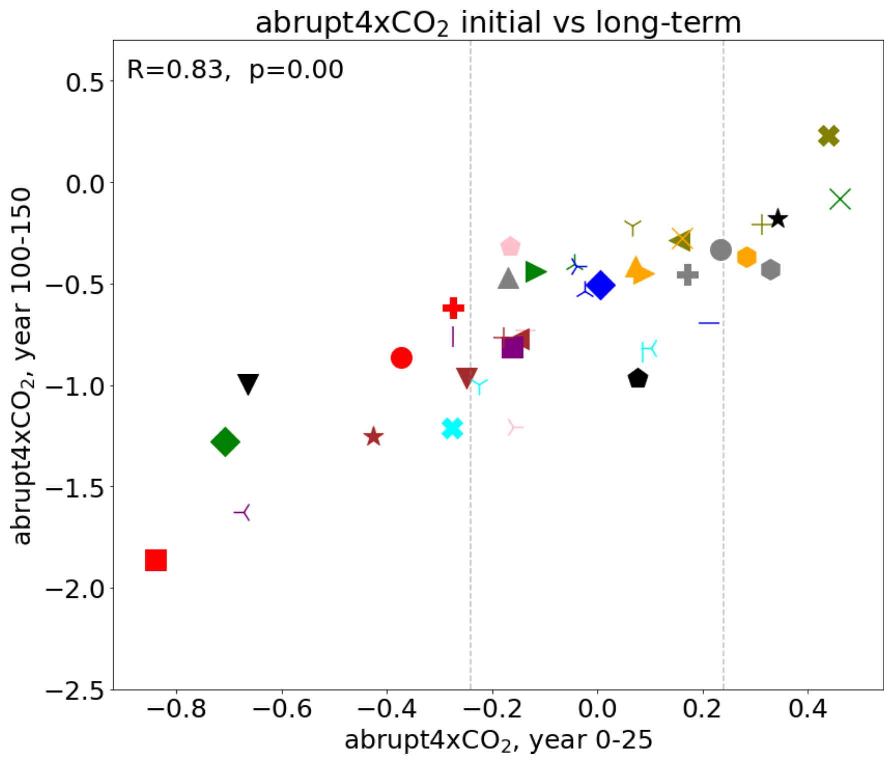

Model name and marker	Model name and marker	Model name and marker	Model name and marker
ACCESS-CM2^{OT}	CESM2-WACCM-FV2	GFDL-ESM4^{*EP}	MIROC-ES2L
ACCESS-ESM1–5*	CIESM	GISS-E2-1-G^{*EP}	MIROC6^{*EP}
BCC-CSM2-MR	CMCC-CM2-SR5^{EP}	GISS-E2-1-H	MPI-ESM1–2-HAM^{OT}
BCC-ESM1*	CNRM-CM6^{*OT}	HadGEM3-GC31-LL*	MPI-ESM1–2-LR^{OT}
CAMS-CMS1–0	CNRM-CM6-HR^{OT}	HadGEM3-GC31-MM	MRI-ESM2*
CanESM5^{*EP}	CNRM-ESM2–1^{OT}	INM-CM4–8	NESM3
CAS-EMS2–0	E3SM^{EP}	INM-CM5–0	NorCPM1^{OT}
CESM2^{*EP}	FGOALS-f3-L	IPSL-CM6A*	SAM0-UNICON^{EP}
CESM2-FV2	FGOALS-g3^{*EP}	KACE-1-0-G	TaiESM1
CESM2-WACCM^{EP}	GFDL-CM4	MCM-UA-1–0	UKESM1-0-LL

Supplementary Figure 1. Overview of CMIP6 models included with the EP and OT categories noted. *Then horizontal axis shows the change in the Indo-Pacific east-west SST gradient in the first 25 years of the abrupt-4xCO_2 experiment, and the vertical axis shows the gradient after 100 years. Adapted from Heede and Fedorov (2021). Note that the OT models used in the analysis are right of the leftmost stippled line: ACCESS-CM2, CNRM-CM6, CNRM-ESM2, CNRM-CM6-HR, MPI-ESM-1-2-HAM, MPI-ESM-1-2-LR, NorCPM1. While the EP models are right of the rightmost stippled line. This SST gradient is defined following Heede and Fedorov (2021) as 80 ^{o}E to 150 ^{o}E minus 180 ^{o}E to 280^{o}E averaged between 5^o S to 5^o N.*

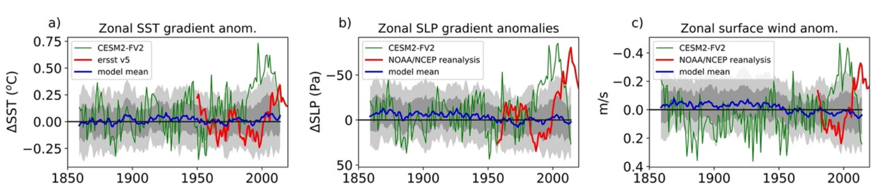

Supplementary Figure 2. As in Fig. 2 but with CESM2-FV2 is highlighted in green to illustrate the strengthening of the Pacific Walker cell simulated by this particular model in the late 20^{th}- early 21^{st} century. Yet, this example is an exception among the models analyzed.

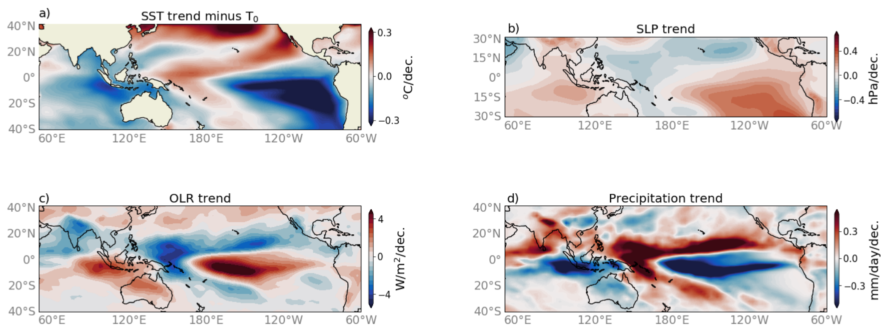

Supplementary Figure 3. As in Fig. 1 but for the CESM2-FV2 (ensemble member r1i1p1f1) historical simulation and a slightly different period (1970-2010).

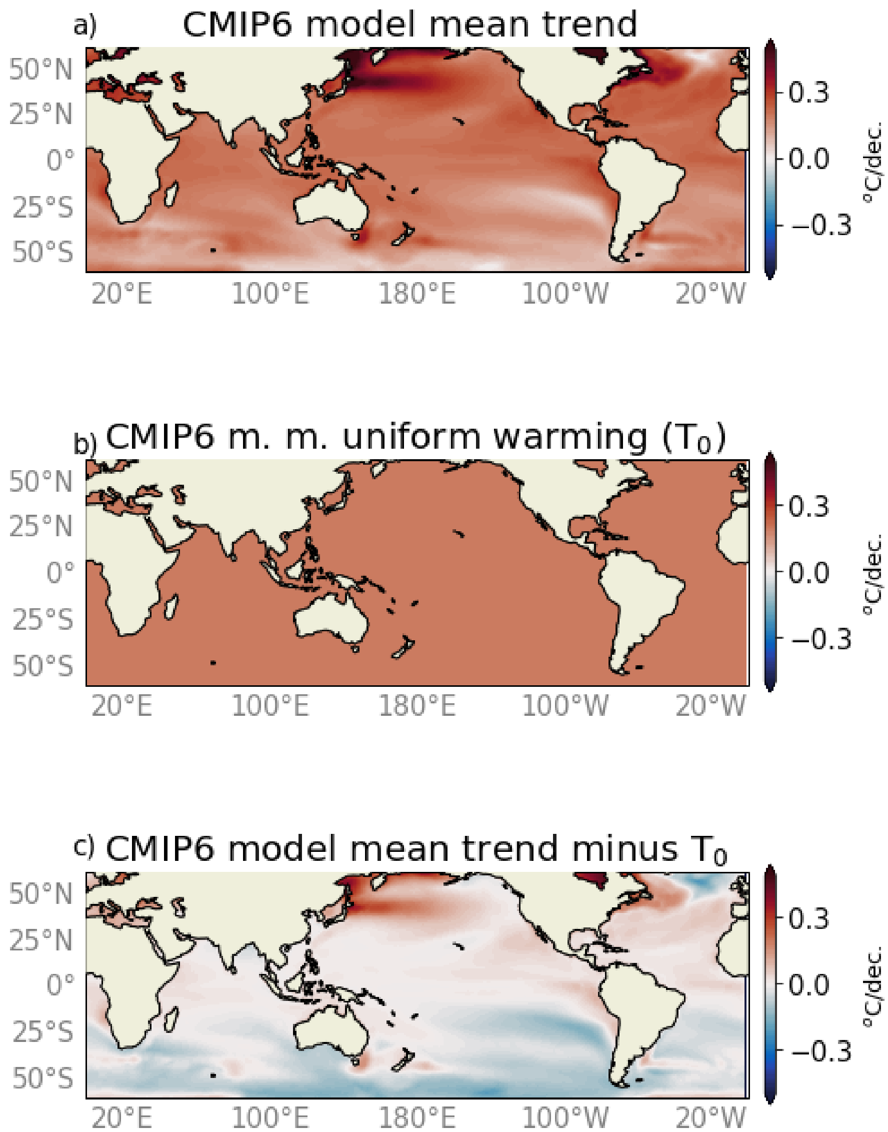

Supplementary Figure 4. *Decomposing CMIP6 multi-model-mean historical SST trends into different components.*

(a) Global map of local SST trends for years 1980-2020. These trends are partitioned into two components: (b) spatially uniform warming trend T_0; and (c) the residual trend pattern once the uniform warming has been subtracted (c.f. Fig. 3d or Suppl Fig. 3d). There is no discernible PDO signal in the multi-model mean sense. Note the preferential warming of the Northern hemisphere in panel (c), but no clear signature along the equator. The last five years (from 2015 to 2020) are obtained from the SSP5-8.5 scenario.

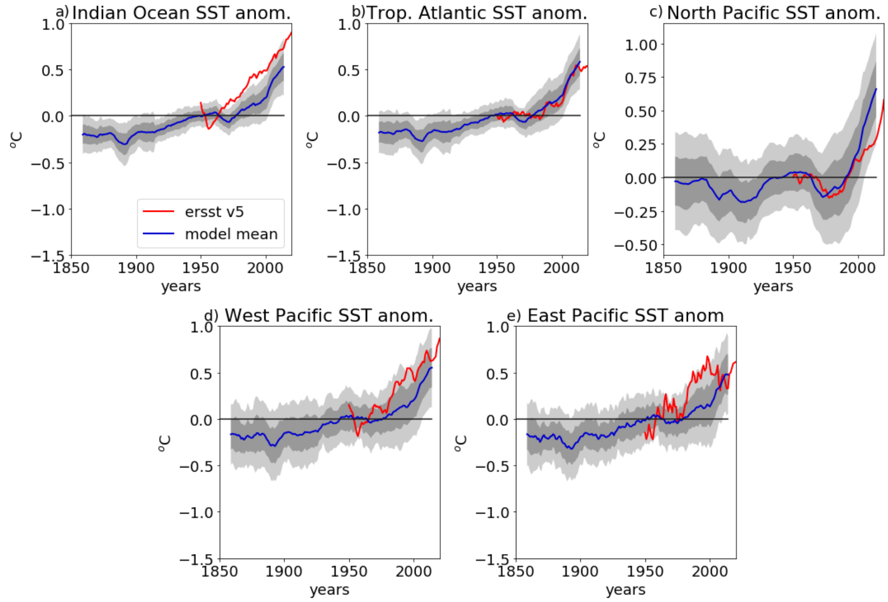

Supplementary Fig 5. Decadal warming trends for different ocean regions in CMIP6 models and observations. *The multi-model mean (in blue) is calculated using one ensemble member for each of 40 different models used. The spread across the models is indicated by dark and light grey shadings (one and two standard deviations, respectively). A 10-year running mean is applied before calculating the spread. To account for mean state biases, all trends are evaluated relative to the 1950-1970 baseline. SST anomalies are estimated for the following regions: (a) Equatorial Indian Ocean: 40° E - 100° E. (b) Equatorial Atlantic: 50° W - 20° W. (c) North Pacific: 120° E to 120° W, 20° N to 65° N. (d) Equatorial West Pacific: 150° E - 180° E. (e) Equatorial East Pacific: 180° E - 80° W. Equatorial variables are averaged between 5° S -5° N.*

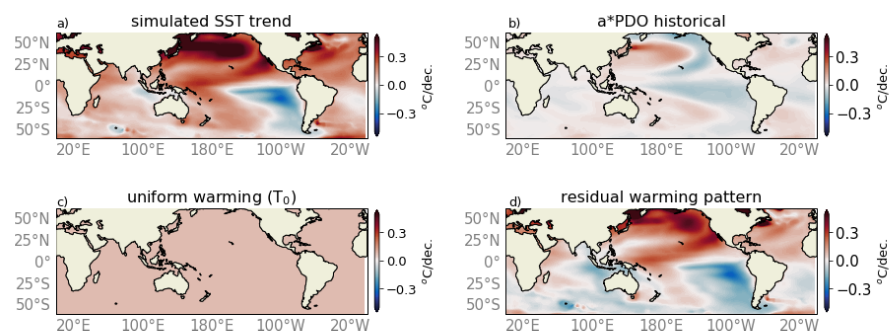

Supplementary Figure 6. *As in Fig. 3 but for the CESM2-FV2 historical simulation (ensemble member r1i1p1f1) and the same period as in Supplementary Fig. 2 (1970-2010). Note apparent similarities with Fig. 3.*

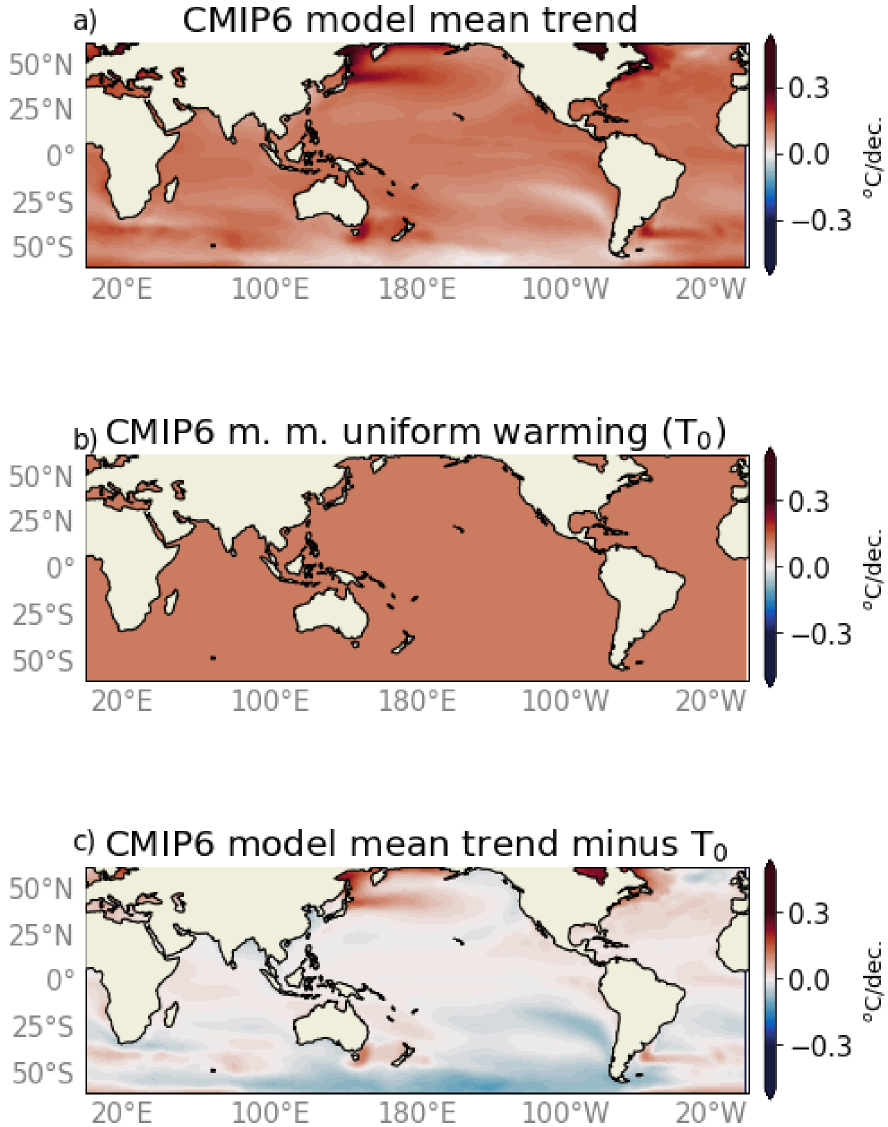

Supplementary Figure 7. *As in Supplementary Fig. 4 but for the time period 1950-2020.*

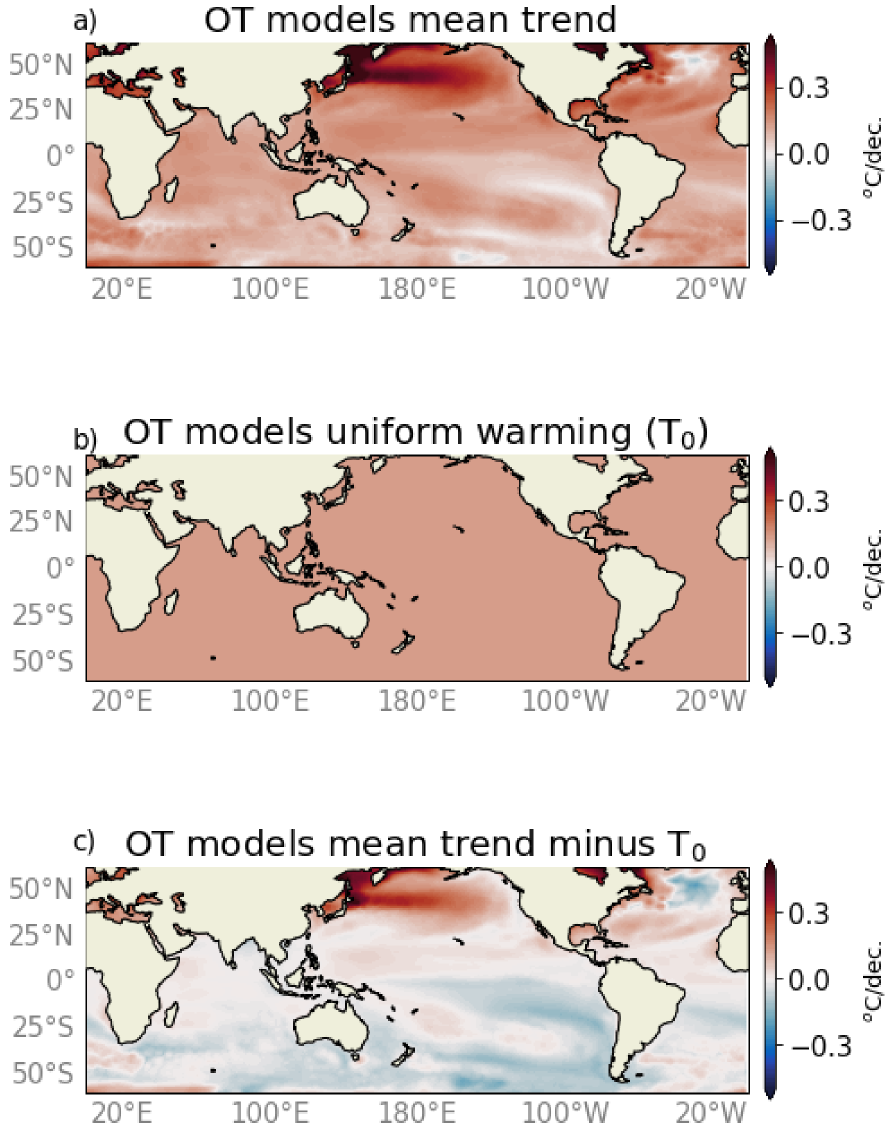

Supplementary Figure 8. *As in Supplementary Fig. 4 but for the OT models only. Panel (c) is reproduced in Fig. 5d but multiplied by four decades.*

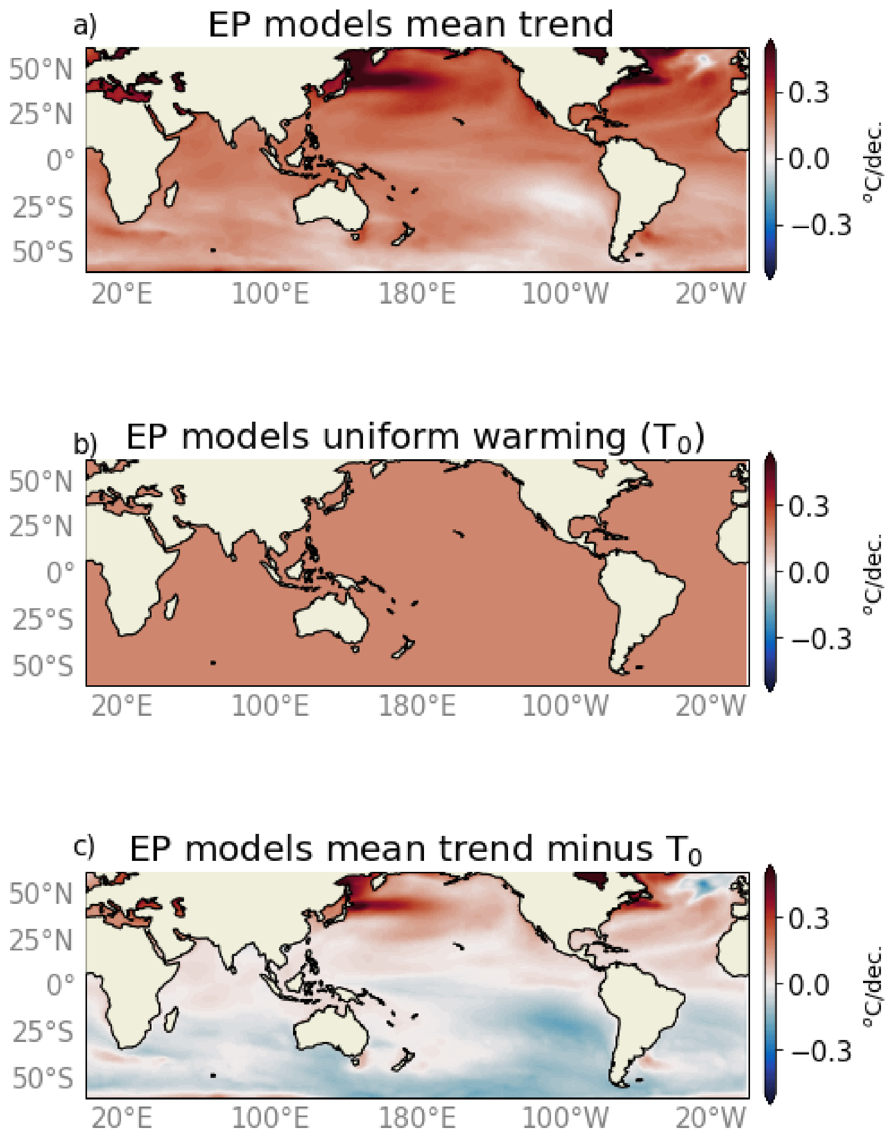

Supplementary Figure 9. *As in Supplementary Fig. 4 but for the EP models only. Panel (c) is reproduced in Fig. 5d but multiplied by four decades.*

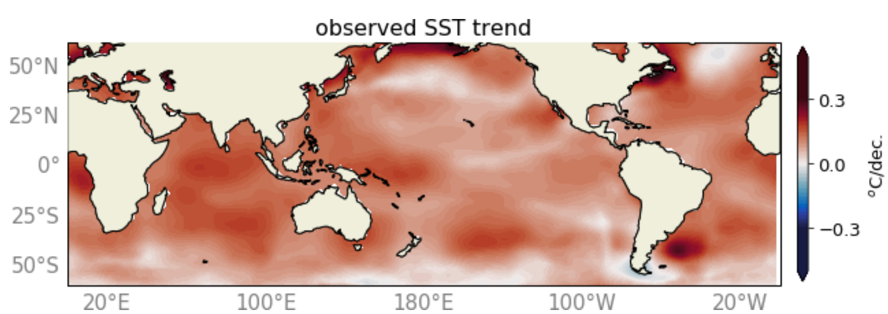

Supplementary Figure 10. *As in Fig. 3a but for a longer time period (1950-2020). Note the enhanced warming of the Indian ocean noted in other studies as well (e.g.Hu and Fedorov 2019), however the trends associated with the weakening of the Walker circulation are much less pronounced, if any.*

Colder eastern equatorial Pacific and stronger Walker cell in the early 21st century: isolating the forced response to global warming

Ulla K. Heede[1]* and Alexey V. Fedorov[1,2]

[1]Department of Earth and Planetary Science, Yale University, New Haven, CT
[2] LOCEAN/IPSL, Sorbonne University, Paris

* Corresponding author: 210 Whitney Avenue, 06511 New Haven CT, ulla.heede@yale.edu

Abstract

Since the early 1990s the Pacific Walker circulation shows a multi-decadal strengthening, contradicting future model projections. Whether this trend, evident in a range of indices especially before the 2015 El Niño, reflects the coupled ocean-atmosphere response to global warming or the negative phase of the Pacific Decadal Oscillation (PDO) remains debated. Here we show that sea surface temperature (SST) trends during 1980-2020 are dominated by three signals: a spatially uniform warming trend, a negative PDO pattern, and a Northern Hemisphere/Indo-West Pacific warming pattern. The latter pattern, which closely resembles the transient ocean thermostat-like response to global warming emerging in a subset of CMIP6 models, shows cooling in the central-eastern Pacific but warming in the western Pacific and tropical Indian ocean. This pattern contributes to the Walker circulation strengthening along with the PDO. Historical simulations appear to underestimate this pattern, contributing to the models' inability to replicate the Walker cell strengthening.

Introduction

The Tropical Pacific modulates the global climate on a broad range on timescales. The easterly trade winds drive equatorial upwelling, the strength of which is controlled by atmospheric zonal circulation – the Pacific Walker cell. The Walker cell is in turn coupled to the Pacific east-west surface temperature gradient via the Bjerknes feedback (Bjerknes 1969). Variations in the strength of the Walker cell occur both on interannual timescales, driving the El Niño Southern Oscillation (ENSO) (McPhaden, Santoso, and Cai 2020), and on decadal timescales, playing a key role in the Pacific Decadal Oscillation (Mantua and Hare 2002). Both ENSO and the PDO have been argued to modulate the rates of surface mean temperature increase in the context of contemporary global warming (England et al. 2014; Kosaka and Xie 2016; Hu and Fedorov 2017). Furthermore, the Pacific Walker cell is sensitive to external forcing, shown both in the paleo context (Fedorov et al. 2015; Shankle et al. 2021) and with contemporary climate change (i.e. Knutson and Manabe, 1995; DiNezio *et al.*, 2009; Heede et al., 2020, 2021).

The majority of Global Climate Models (GCMs) analyzed as part of the Coupled Model Intercomparison Project (CMIP) indicate that the tropical Pacific Walker cell will slow down in the future, in response to increasing radiative forcing, which will be accompanied by the establishment of the eastern equatorial Pacific warming pattern (DiNezio et al. 2009; 2012; Xie et al. 2010; Kociuba and Power 2015, 5; Coats and Karnauskas 2017; Heede and Fedorov 2021). The development of this warming pattern can be explained by several contributing factors, including enhanced atmospheric stratification due to increase in latent heat release in the mid to upper troposphere (Knutson and Manabe 1995; Held and Soden 2006; Vecchi and Soden 2007), the lesser ability of the colder eastern Pacific to balance increased radiative forcing with latent heat release compared to the warmer western Pacific (Merlis and Schneider 2011; Heede et al. 2020), positive marine boundary layer cloud feedbacks in the eastern Pacific (Erfani and Burls 2019), and enhanced extra-tropical warming and/or slowdown of the oceanic subtropical cells (McCreary Jr and Lu 1994; Burls and Fedorov 2014; Heede et al. 2020; 2021; Sun et al. 2004).

These GCM results have motivated studies looking for a similar eastern equatorial Pacific warming pattern and Walker cell slowdown in the observed record. Several studies argued that the Walker cell may have shown a long-term weakening trend throughout the 20th century (Vecchi et al. 2006; Tokinaga et al. 2012). However, these findings contradict other studies suggesting that the Pacific east-west SST gradient has increased over the 20th century (Solomon and Newman 2012; Seager et al. 2019). During the satellite era, when some of the uncertainties are greatly reduced, a robust multi-decadal strengthening of Pacific trade winds has been observed (Meng et al. 2012; Sohn et al. 2013; Luo et al. 2015; Ma and Zhou 2016).

This apparent discrepancy between future projections and the recently observed trends, and the inability of CMIP models to capture the observed trends, has brought the reliability and robustness of the future projections of a weaker Walker into question (Kociuba and Power 2015; Seager et al. 2022). A related key issue has emerged: does the observed trend reflect the negative phase of the Pacific Decadal Oscillation (PDO) – a part of natural climate variability which the models do not necessarily capture well (Douville et al. 2015; McGregor et al. 2018)? A series of studies have argued that natural decadal variability may indeed play a role in the current trends and explain a part of the observed trend in the Pacific (Chung et al. 2019; Wu et al. 2021; Watanabe et al. 2020).

Simultaneously, however, studies documented the existence of a transient response to global warming in GCMs involving a strengthening of the Walker cell, akin to an ocean thermostat-type response first documented by Clement et al. (1996), Sun and Liu (1996) and (Seager and Murtugudde 1997). Using a simple coupled model Seager *et al.* (2019) argued that a forced thermostat-type response to rising greenhouse gas concentrations may be consistent with the observed trends. However, in contrast to the original ideas of Clement *et al.* (1996) who used a Zebiak-Cane model (1987) with a fixed ocean mean state, this ocean thermostat must be a transient phenomenon as the subsurface ocean gradually warms thus limiting the effect of enhanced upwelling. Heede et al. (2020,2021) have shown that this transient response can maintain a stronger Walker cell for about half-a-century or even longer depending on the rate of change of the forcing (abrupt versus gradual). Additionally, a study nudging Indian ocean temperatures towards observed values in a GCM likewise showed an Indo-Pacific Walker cell strengthening (Zhang et al. 2019). Together, these studies suggest the possibility that the current trends may in part be driven by a transient response to global warming, as the far western equatorial Pacific and the Indian Ocean warm faster than the central-eastern Pacific, causing a stronger Pacific Walker cell.

An overarching goal of the present study is to provide new insights into the recent decadal strengthening of the Walker circulation in the context of ongoing climate change. Using a broad range of indices based on different physical variables updated with the most recent data, including their spatial trends, reveal nuances a single index cannot capture and can help reduce uncertainty concerning whether a trend exceeds natural variability or not. Our further goal is to extract a pattern from the observed SST trends that is not associated with either the PDO signal or the uniform warming trend, and to compare this pattern and related Walker circulation changes to those generated by CMIP6 models. We refer to this residual pattern, presumably anthropogenically forced, as the Northern Hemisphere/Indo-West Pacific warming pattern (NH-IWP). We then compare it to the transient ocean-thermostat pattern simulated by a subset of CMIP6 models in a range of realistic and idealized global warming simulations while discussing the key mechanisms involved.

Methods

Pacific Walker circulation indices and decomposition of SST trends

To evaluate recent changes to the Pacific Walker cell, we use eight indices based on different physical variables all reflecting the strength of the Walker circulation from a combination of satellite, reanalysis and blended datasets. The datasets used to define these metrics are summarized in Supplementary Table 1.

To compare the observed SST trends of the last 40 years with patterns associated with natural decadal variability in the Pacific, we define the PDO largely following d'Orgeville and Peltier (2007). We smooth the SST data using a 5-year rolling mean to eliminate shorter interannual variability. Then we take SST anomalies from 1920 until 2021 and compute the first and second EOFs for the North Pacific region defined as 120° E to 260° E, 20° N to 65° N. To obtain a global PDO pattern, we regress 5-year smoothed SST data for the same period onto the principal component timeseries corresponding to the 2nd EOF for the North Pacific.

Next, we calculate a spatially uniform linear warming trend T_0, in °C/decade, from 1980 to 2021, and subtract it from the observed full trend pattern to get spatially varying anomalies in the region 65° S to 65° N. We then compute a spatial linear regression of those anomalies onto the already obtained PDO pattern by computing coefficient a, having units of decade^{-1}, which minimizes the difference between the PDO pattern multiplied by a and these anomalies. The residual, obtained by subtracting the a*PDO from the anomalies, is not associated with the PDO pattern nor with uniform global warming. In summary, the trends are represented as:

$$Trends_{lat,lon} = T_0 + a \cdot PDO_{lat,lon} + residual_{lat,lon}$$

The CMIP6 archive

To compare the observed trends with a broad range of CMIP6 models, we consider 40 different models from the CMIP6 archive (Eyring et al. 2016), as listed in Supplementary Figure 1, for which surface temperature (ts), sea level pressure (psl) and surface winds (uas) are available for the historical simulation. To give each model equal weight, we utilize only one ensemble member per model.

Finally, we select a subset of models that have been identified as having a strong transient ocean-thermostat-like (OT) response to global warming in idealized CO_2 scenarios (here referred to as OT models, listed in Supplementary Fig 1). They are selected based on the criterion that their Indo-Pacific SST gradient increases by at least 0.25 °C relative to the piControl experiment during the first 25 years of the abrupt-4xCO_2 simulation. Another model subset used includes models that develop a strong eastern equatorial Pacific (EP) warming pattern (see Supplementary Fig 1).

Furthermore, we identify one model, CESM2-FV2, which is an outlier among CMIP6 models but which has a strong late 20th century Walker circulation strengthening trend, as measured by the zonal SST gradient strength, comparable to the observed trend, yet it is not part of the OT subset. For CESM2-FV2, we also decompose the 40-year SST trend pattern simulated by this model into different components, as done for the observations, and compare with the historical data.

Results

40-year trends of the Pacific Walker circulation

Fig. 1 shows a clear decadal strengthening of the Walker circulation, as reflected in a variety of physical variables, that is robust across all indices since the 1990s. In most variables, the trend appears to be strongest between the El Niño events of 1997 and 2015. The trend is more pronounced in the SLP gradient than the SST gradient. After the year 2016, the trend does not continue for the majority of indices. For some indices (SLP, SLH), it appears to reverse the sign, while for some other indices (OLR and Omega), the trend plateaus. Nevertheless, for the zonal equatorial current speed the trend continues after 2015, showing no reversal or plateau. These differences preclude us from concluding whether the Walker cell strengthening trend has resumed or subsided after the El Niño of 2015.

Looking at spatial changes contributing to the Walker circulation trends, we highlight a pronounced SST cooling in the Pacific SST since the 1980s that is located primarily in the eastern equatorial Pacific and the region south of the equator adjacent to South America (Fig. 1h). SLP trends show decreasing pressure over the Maritime continent but increasing pressure in the central-eastern equatorial Pacific. Correspondingly, precipitation and OLR trends show an increase in precipitation (decrease in OLR) over the Maritime continent, and a decrease in precipitation (increase in OLR) across the Pacific (Figs. 1). All these changes are indicative of the Walker circulation intensification (and the general strengthening of Pacific trade winds).

Comparison between the observed and CMIP6 model Walker cell trends

Comparing three critical indices for the Walker cell (zonal SST gradient, SLP gradient, and surface winds along the equator) in Fig. 2, we find that the observed anomalies in the SST gradient reach, but does not exceed two standard deviations of CMIP6 model spread, while both the SLP gradient and the surface wind index do exceed two standard deviations of the CMIP6 spread during the peak of the Walker circulation strengthening trend, indicating that the observed Walker cell trends cannot be replicated by CMIP6 models at large.

We have identified only one model, which has a late 20th century Walker cell strengthening trend which *exceeds* (albeit slightly) the observed trend between 1970 and 2019 – CESM2-FV2 as shown in Supplementary Fig 2. As evident in Supplementary Fig. 3, this model has patterns of trends in the tropical Pacific qualitatively similar to the observed in Fig. 2. However, at the same time this model shows cooling in the Indian ocean and a weaker warming in the South Pacific, driving sea level pressure anomalies in those regions that differ from the observed trends.

Decomposing SST trend pattern into a PDO signal and a residual signal

Fig. 3 shows a decomposition of the observed SST trends (as a function of latitude and longitude) into the PDO signal, a spatially uniform warming and a non-PDO residual. These three signals have all comparable magnitudes. Importantly, the eastern-central Pacific cooling persists in the residual SST pattern (Fig. 3d). In addition, the residual pattern shows a clear hemispheric asymmetry with enhanced warming in the northern hemisphere and cooling in the southern hemisphere as well as a stronger SST gradient between the Pacific and Indian oceans. We refer to this pattern as the Northern Hemisphere/Indo-West Pacific warming pattern (NH-IWP). The origin of this pattern will be described next.

Comparison of SST patterns between observations and CMIP6 models

To understand the origin of the NH-IWP warming pattern (i.e. the non-PDO residual), we turn to the subset of CMIP6 models with a strong OT response (Methods). Fig. 4 compares the observed residual trends to the OT model SST anomalies across idealized and historical experiments. The residual trend pattern looks remarkably similar to the first decades of the abrupt-4xCO_2 response to the forcing of OT models, both in terms of the southern hemisphere cooling and tropical Indo-Pacific temperature gradient (Fig. 4b). Qualitatively, this pattern also looks similar in the gradual 1pctCO_2 and historical simulations (Fig. 4c,d), even though the Indian ocean warming is weaker, and hence the resultant strengthening of the Indo-Pacific temperature gradient is smaller than in the observations. Overall, the similarity of the NH-IWP pattern and the transient OT response in this subset of models suggests that this pattern may be part of the climate system forced response to radiative forcing.

In the CMIP6 model mean across all 40 models, the Pacific cooling signal is absent (Supplementary Fig. 4). Conversely, there is a strong localized warming in the subtropical gyre region of the North Pacific, which does not appear in the observed residual trend, once the PDO signal is subtracted (Fig. 3d).

Supplementary Fig. 5 compares warming SST trends averaged for different regions of the tropical ocean basins in the observations and in CMIP6. It is evident that the CMIP6 models consistently underestimate warming in the Indian Ocean by about 0.3 K on average since 1950 with the observed trend outside two standard deviations of the CMIP6 model mean trend. Simultaneously, the CMIP6 models overestimate the North Pacific warming by about 0.3 K between 1970 and 2000. The observed Atlantic warming is captured well by the models, while both the East and West Pacific warming is, on average, slightly underestimated by the models, but within two standard deviations.

For the only model (CESM2-FV2) in which the Walker circulation trend exceeds the observed trend, we complete the same trend partitioning at in Fig. 3 but for the period of its historical simulation during which the Walker circulation increase is the strongest (Supplementary Fig. 6). For this particular model, the PDO and uniform warming signals are generally similar to the observations (Fig. 3). The residual warming trend, however, has both similarities and differences. In particular, the ocean cools in the eastern equatorial Pacific and off the South American coast, strengthening the east-west Pacific SST gradient. However, there is no enhanced Indian Ocean warming relative to the mean warming, which is markedly different from the observations. The North Pacific warming and interhemispheric asymmetry appear stronger in CESM2-FV2 than in the CMIP6 average.

Discussion and conclusions

A multi-variable assessment of the Pacific Walker circulation changes since 1980 shows a robust decadal strengthening trend, particularly pronounced from the early 1990s to 2015. This trend is accompanied by a central-eastern Pacific SST cooling along equator and off the coast of South America, a pronounced deepening of low pressure and increased precipitation over the Maritime continent, and a precipitation decrease over most of the equatorial Pacific Ocean.

The full pattern of ocean warming share some similarities with the negative PDO pattern, but is distinct from the PDO pattern in two ways: enhanced warming of the northern hemisphere and of the Indian Ocean. This is highlighted by our decomposition of the signal into a spatially uniform warming, the PDO signal, and a non-PDO residual. It is the latter pattern that is characterized by an enhanced NH-IWP warming. All three signals have similar magnitudes. Consequently, the increase in the equatorial Indo-Pacific SST gradient and the increased hemispheric asymmetry compared to the PDO signal suggest that the recently observed decadal trends in the Pacific Walker circulation cannot be explained solely by the transition from a positive to a negative PDO phase.

Indeed, the residual trend pattern that we have isolated in the observations (full trend minus the uniform warming and the PDO), i.e. the NH-IWP pattern, generally resembles the transient pattern that emerges in the Indo-Pacific during the first decades of the abrupt-4xCO_2 experiment among the OT model subset of CMIP6 models. Crucially however, in more gradual forcing scenarios the OT models capture this strong Indo-Pacific SST pattern only partially (having too weak Indian ocean warming), which raises the question whether CMIP models at large are missing or underestimating the strengthening of the Walker cell as part of the transient forced response to global warming. Eventually, the weakening of the Walker cell, while delayed by the transient response, is expected by the end of the 21st century (Xie et al. 2010; DiNezio, Vecchi, and Clement 2013; Kang et al. 2020; Heede and Fedorov 2021; Wu et al. 2021). However, coupled GCM experiments show that the timing and magnitude of the future weakening depends on the strength of the transient ocean thermostat-like response to global warming (Heede and Fedorov 2021; Lu et al. 2021), which on the whole appears to be underestimated by the CMIP6 models, especially in the late 20th and early 21st century, raising questions about whether the models' prediction of accelerated future Pacific warming are fully realistic.

The tendency to underestimate Indian Ocean warming appears to be a general issue among the CMIP6 models for which the observed trend lies outside two standard deviations of the average. The models' failure to capture the enhanced Indian Ocean warming in particular could explain why the models largely fail to capture the sea-level pressure and surface wind trends.

The models' overestimating the North Pacific warming is principally related to the simulated strong warming in the center of the northern subtropical gyre. This pattern is evident in the multi-model mean since 1950 (Supplementary Fig. 7) and across both OT and EP models (Supplementary Figs. 8 and 9). This trend is also evident in the observations, but only since 1980, which correlates with the PDO signal (Supplementary Fig. 10). Therefore, it is difficult to assess the exact extent that the observed North Pacific warming is influenced by global warming, but the strong south-north asymmetry of the pattern suggest that global warming does play an important role.

Among climate models analyzed, we find only one model (CESM2-FV2) that shows a late 20th century trend, similar to the observed in term of the magnitude of changes in the east-west equatorial SST gradient. In this model we see a qualitatively similar PDO pattern and a similar amplification of northern hemisphere warming in addition to the PDO signal. However, while this hemispheric asymmetry is even greater in the model than in the observations, the Indian ocean shows cooling relative to the mean warming. The leads to somewhat different spatial trend patterns in SLP and precipitation, driven by the strong north-south SST gradient in CESM2-FV2, rather than the zonal Indo-Pacific gradient as in the observations. Nevertheless, the residual NH IWP pattern (albeit modified) has clear similarities with that in the observations, and it is the simultaneous occurrence of this pattern and the negative PDO that enables the strong strengthening trend of the Walker circulation in this model.

Wu et al. (2021) have argued that model simulations with enough ensemble members are able to capture the observed strengthening of the Pacific Walker circulation trends by generating ensemble members that produce a sufficiently strong negative phase of the PDO. However, as we have shown in this paper, the PDO alone is not sufficient to describe the spatial structure of the observed trends. Another mode is also needed, i.e. the NH-IWP warming pattern, which looks like a transient forced response of the system. It is also worth noting, as illustrated here for the CEMS2-FV2 model, that it may be possible to replicate the observed changes in the Walker circulation without capturing the underlying trans-basin warming trends, which could influence the magnitude and duration of the Walker cell transient response. The inability of CMIP6 models to capture the observed differences in the warming rates across tropical ocean basins could have implications for the models' ability to accurately predict the timing of the emergence of a weaker Pacific Walker circulation (i. e. Ying *et al.*, 2022) and the magnitude of its future weakening.

Competing interests statement

The authors declare no competing interests.

Data sharing statement

All CMIP6 data is available on https://esgf-node.llnl.gov/search/cmip6/. All observed data is available stated in Supplementary Table 1. All code used for data analysis and figures is available upon request and will be released on github upon publication.

Funding statement

U.K.H. is supported by a NASA FINESST Fellowship (80NSSC20K1634). A.V.F. is supported by grants from NASA (80NSSC21K0558) and NOAA (NA20OAR4310377). Additional funding is provided by the ARCHANGE project (ANR-18-MPGA-0001, France). We also acknowledge a generous gift to Yale University from T. Sandoz. The funders had no role in study design, data collection and analysis, decision to publish or preparation of the manuscript.

References

Bjerknes, Jakob. 1969. 'Atmospheric Teleconnections from the Equatorial Pacific'. *Monthly Weather Review* 97 (3): 163–72.

Burls, N. J., and A. V. Fedorov. 2014. 'What Controls the Mean East–West Sea Surface Temperature Gradient in the Equatorial Pacific: The Role of Cloud Albedo'. *Journal of Climate* 27 (7): 2757–78.

Chung, Eui-Seok, Axel Timmermann, Brian J. Soden, Kyung-Ja Ha, Lei Shi, and Viju O. John. 2019. 'Reconciling Opposing Walker Circulation Trends in Observations and Model Projections'. *Nature Climate Change* 9 (5): 405–12. https://doi.org/10.1038/s41558-019-0446-4.

Clement, Amy C., Richard Seager, Mark A. Cane, and Stephen E. Zebiak. 1996. 'An Ocean Dynamical Thermostat'. *Journal of Climate* 9 (9): 2190–96.

Coats, S., and K. B. Karnauskas. 2017. 'Are Simulated and Observed Twentieth Century Tropical Pacific Sea Surface Temperature Trends Significant Relative to Internal Variability?' *Geophysical Research Letters* 44 (19): 9928–37.

DiNezio, Pedro N., Amy C. Clement, Gabriel A. Vecchi, Brian J. Soden, Benjamin P. Kirtman, and Sang-Ki Lee. 2009. 'Climate Response of the Equatorial Pacific to Global Warming'. *Journal of Climate* 22 (18): 4873–92.

DiNezio, Pedro N., Ben P. Kirtman, Amy C. Clement, Sang-Ki Lee, Gabriel A. Vecchi, and Andrew Wittenberg. 2012. 'Mean Climate Controls on the Simulated Response of ENSO to Increasing Greenhouse Gases'. *Journal of Climate* 25 (21): 7399–7420. https://doi.org/10.1175/JCLI-D-11-00494.1.

DiNezio, Pedro N., Gabriel A. Vecchi, and Amy C. Clement. 2013. 'Detectability of Changes in the Walker Circulation in Response to Global Warming'. *Journal of Climate* 26 (12): 4038–48.

Douville, H., A. Voldoire, and O. Geoffroy. 2015. 'The Recent Global Warming Hiatus: What Is the Role of Pacific Variability?' *Geophysical Research Letters* 42 (3): 880–88. https://doi.org/10.1002/2014GL062775.

England, Matthew H., Shayne McGregor, Paul Spence, Gerald A. Meehl, Axel Timmermann, Wenju Cai, Alex Sen Gupta, Michael J. McPhaden, Ariaan Purich, and Agus Santoso. 2014. 'Recent Intensification of Wind-Driven Circulation in the Pacific and the Ongoing Warming Hiatus'. *Nature Climate Change* 4 (3): 222–27.

Erfani, Ehsan, and Natalie J. Burls. 2019. 'The Strength of Low-Cloud Feedbacks and Tropical Climate: A CESM Sensitivity Study'. *Journal of Climate* 32 (9): 2497–2516.

Eyring, Veronika, Sandrine Bony, Gerald A. Meehl, Catherine A. Senior, Bjorn Stevens, Ronald J. Stouffer, and Karl E. Taylor. 2016. 'Overview of the Coupled Model Intercomparison Project Phase 6 (CMIP6) Experimental Design and

Organization'. *Geoscientific Model Development* 9 (5): 1937–58. https://doi.org/10.5194/gmd-9-1937-2016.

Fedorov, Alexey V., Natalie J. Burls, Kira T. Lawrence, and Laura C. Peterson. 2015. 'Tightly Linked Zonal and Meridional Sea Surface Temperature Gradients over the Past Five Million Years'. *Nature Geoscience* 8 (12): 975–80.

Heede, Ulla, and Alexey Fedorov. 2021. 'Eastern Equatorial Pacific Warming Delayed by Aerosols and Thermostat Response to CO2'.

Heede, Ulla K., Alexey V. Fedorov, and Natalie J. Burls. 2020. 'Timescales and Mechanisms for the Tropical Pacific Response to Global Warming: A Tug of War between the Ocean Thermostat and Weaker Walker'. *Journal of Climate*, April. https://doi.org/10.1175/JCLI-D-19-0690.1.

———. 2021. 'A Stronger versus Weaker Walker: Understanding Model Differences in Fast and Slow Tropical Pacific Responses to Global Warming'. *Climate Dynamics*, 1–18.

Held, Isaac M., and Brian J. Soden. 2006. 'Robust Responses of the Hydrological Cycle to Global Warming'. *Journal of Climate* 19 (21): 5686–99.

Hu, Shineng, and Alexey V. Fedorov. 2017. 'The Extreme El Niño of 2015–2016 and the End of Global Warming Hiatus'. *Geophysical Research Letters* 44 (8): 3816–24. https://doi.org/10.1002/2017GL072908.

Kang, Sarah M., Shang-Ping Xie, Yechul Shin, Hanjun Kim, Yen-Ting Hwang, Malte F. Stuecker, Baoqiang Xiang, and Matt Hawcroft. 2020. 'Walker Circulation Response to Extratropical Radiative Forcing'. *Science Advances* 6 (47): eabd3021. https://doi.org/10.1126/sciadv.abd3021.

Knutson, Thomas R., and Syukuro Manabe. 1995. 'Time-Mean Response over the Tropical Pacific to Increased C02 in a Coupled Ocean-Atmosphere Model'. *Journal of Climate* 8 (9): 2181–99.

Kociuba, Greg, and Scott B. Power. 2015. 'Inability of CMIP5 Models to Simulate Recent Strengthening of the Walker Circulation: Implications for Projections'. *Journal of Climate* 28 (1): 20–35.

Kosaka, Yu, and Shang-Ping Xie. 2016. 'The Tropical Pacific as a Key Pacemaker of the Variable Rates of Global Warming'. *Nature Geoscience* 9 (9): 669–73.

Lu, Kezhou, Jie He, Boniface Fosu, and Maria Rugenstein. 2021. 'Mechanisms of Fast Walker Circulation Responses to CO2 Forcing'. *Geophysical Research Letters* 48 (23): e2021GL095708. https://doi.org/10.1029/2021GL095708.

Luo, Yiyong, Jian Lu, Fukai Liu, and Wei Liu. 2015. 'Understanding the El Niño-like Oceanic Response in the Tropical Pacific to Global Warming'. *Climate Dynamics* 45 (7–8): 1945–64.

Ma, Shuangmei, and Tianjun Zhou. 2016. 'Robust Strengthening and Westward Shift of the Tropical Pacific Walker Circulation during 1979–2012: A Comparison of 7 Sets of Reanalysis Data and 26 CMIP5 Models'. *Journal of Climate* 29 (9): 3097–3118.

Mantua, Nathan J., and Steven R. Hare. 2002. 'The Pacific Decadal Oscillation'. *Journal of Oceanography* 58 (1): 35–44. https://doi.org/10.1023/A:1015820616384.

McCreary Jr, Julian P., and Peng Lu. 1994. ‘Interaction between the Subtropical and Equatorial Ocean Circulations: The Subtropical Cell’. *Journal of Physical Oceanography* 24 (2): 466–97.

McGregor, Shayne, Malte F. Stuecker, Jules B. Kajtar, Matthew H. England, and Mat Collins. 2018. ‘Model Tropical Atlantic Biases Underpin Diminished Pacific Decadal Variability’. *Nature Climate Change* 8 (6): 493–98. https://doi.org/10.1038/s41558-018-0163-4.

McPhaden, Michael J., Agus Santoso, and Wenju Cai. 2020. *El Niño Southern Oscillation in a Changing Climate*. Vol. 253. John Wiley & Sons.

Meng, Qingjia, Mojib Latif, Wonsun Park, Noel S. Keenlyside, Vladimir A. Semenov, and Thomas Martin. 2012. ‘Twentieth Century Walker Circulation Change: Data Analysis and Model Experiments’. *Climate Dynamics* 38 (9–10): 1757–73.

Merlis, Timothy M., and Tapio Schneider. 2011. ‘Changes in Zonal Surface Temperature Gradients and Walker Circulations in a Wide Range of Climates’. *Journal of Climate* 24 (17): 4757–68.

Orgeville, Marc d’, and W. Richard Peltier. 2007. ‘On the Pacific Decadal Oscillation and the Atlantic Multidecadal Oscillation: Might They Be Related?’ *Geophysical Research Letters* 34 (23). https://doi.org/10.1029/2007GL031584.

Seager, Richard, Mark Cane, Naomi Henderson, Dong-Eun Lee, Ryan Abernathey, and Honghai Zhang. 2019. ‘Strengthening Tropical Pacific Zonal Sea Surface Temperature Gradient Consistent with Rising Greenhouse Gases’. *Nature Climate Change* 9 (7): 517–22.

Seager, Richard, Naomi Henderson, and Mark Cane. 2022. ‘Persistent Discrepancies between Observed and Modeled Trends in the Tropical Pacific Ocean’. *Journal of Climate* 1 (aop): 1–41. https://doi.org/10.1175/JCLI-D-21-0648.1.

Seager, Richard, and Ragu Murtugudde. 1997. ‘Ocean Dynamics, Thermocline Adjustment, and Regulation of Tropical SST’. *Journal of Climate* 10 (3): 521–34.

Shankle, Madison G., Natalie J. Burls, Alexey V. Fedorov, Matthew D. Thomas, Wei Liu, Donald E. Penman, Heather L. Ford, Peter H. Jacobs, Noah J. Planavsky, and Pincelli M. Hull. 2021. ‘Pliocene Decoupling of Equatorial Pacific Temperature and PH Gradients’. *Nature* 598 (7881): 457–61. https://doi.org/10.1038/s41586-021-03884-7.

Sohn, B. J., Sang-Wook Yeh, Johannes Schmetz, and Hwan-Jin Song. 2013. ‘Observational Evidences of Walker Circulation Change over the Last 30 Years Contrasting with GCM Results’. *Climate Dynamics* 40 (7): 1721–32. https://doi.org/10.1007/s00382-012-1484-z.

Solomon, Amy, and Matthew Newman. 2012. ‘Reconciling Disparate Twentieth-Century Indo-Pacific Ocean Temperature Trends in the Instrumental Record’. *Nature Climate Change* 2 (9): 691–99. https://doi.org/10.1038/nclimate1591.

Sun, De-Zheng, and Zhengyu Liu. 1996. ‘Dynamic Ocean-Atmosphere Coupling: A Thermostat for the Tropics’. *Science* 272 (5265): 1148–50.

Sun, De-Zheng, Tao Zhang, and Sang-Ik Shin. 2004. ‘The Effect of Subtropical Cooling on the Amplitude of ENSO: A Numerical Study’. *Journal of Climate* 17 (19): 3786–98. https://doi.org/10.1175/1520-0442(2004)017<3786:TEOSCO>2.0.CO;2.

Tokinaga, Hiroki, Shang-Ping Xie, Axel Timmermann, Shayne McGregor, Tomomichi Ogata, Hisayuki Kubota, and Yuko M. Okumura. 2012. ‘Regional Patterns of Tropical Indo-Pacific Climate Change: Evidence of the Walker Circulation Weakening’. *Journal of Climate* 25 (5): 1689–1710.

Vecchi, Gabriel A., and Brian J. Soden. 2007. ‘Global Warming and the Weakening of the Tropical Circulation’. *Journal of Climate* 20 (17): 4316–40.

Vecchi, Gabriel A., Brian J. Soden, Andrew T. Wittenberg, Isaac M. Held, Ants Leetmaa, and Matthew J. Harrison. 2006. ‘Weakening of Tropical Pacific Atmospheric Circulation Due to Anthropogenic Forcing’. *Nature* 441 (7089): 73–76.

Watanabe, Masahiro, Jean-Louis Dufresne, Yu Kosaka, Thorsten Mauritsen, and Hiroaki Tatebe. 2020. ‘Enhanced Warming Constrained by Past Trends in Equatorial Pacific Sea Surface Temperature Gradient’. *Nature Climate Change*, October, 1–5. https://doi.org/10.1038/s41558-020-00933-3.

Wu, Mingna, Tianjun Zhou, Chao Li, Hongmei Li, Xiaolong Chen, Bo Wu, Wenxia Zhang, and Lixia Zhang. 2021. ‘A Very Likely Weakening of Pacific Walker Circulation in Constrained Near-Future Projections’. *Nature Communications* 12 (1): 6502. https://doi.org/10.1038/s41467-021-26693-y.

Xie, Shang-Ping, Clara Deser, Gabriel A. Vecchi, Jian Ma, Haiyan Teng, and Andrew T. Wittenberg. 2010. ‘Global Warming Pattern Formation: Sea Surface Temperature and Rainfall’. *Journal of Climate* 23 (4): 966–86.

Ying, Jun, Matthew Collins, Wenju Cai, Axel Timmermann, Ping Huang, Dake Chen, and Karl Stein. 2022. ‘Emergence of Climate Change in the Tropical Pacific’. *Nature Climate Change*, March, 1–9. https://doi.org/10.1038/s41558-022-01301-z.

Zhang, Lei, Weiqing Han, Kristopher B. Karnauskas, Gerald A. Meehl, Aixue Hu, Nan Rosenbloom, and Toshiaki Shinoda. 2019. ‘Indian Ocean Warming Trend Reduces Pacific Warming Response to Anthropogenic Greenhouse Gases: An Interbasin Thermostat Mechanism’. *Geophysical Research Letters* 46 (19): 10882–90.

Figures

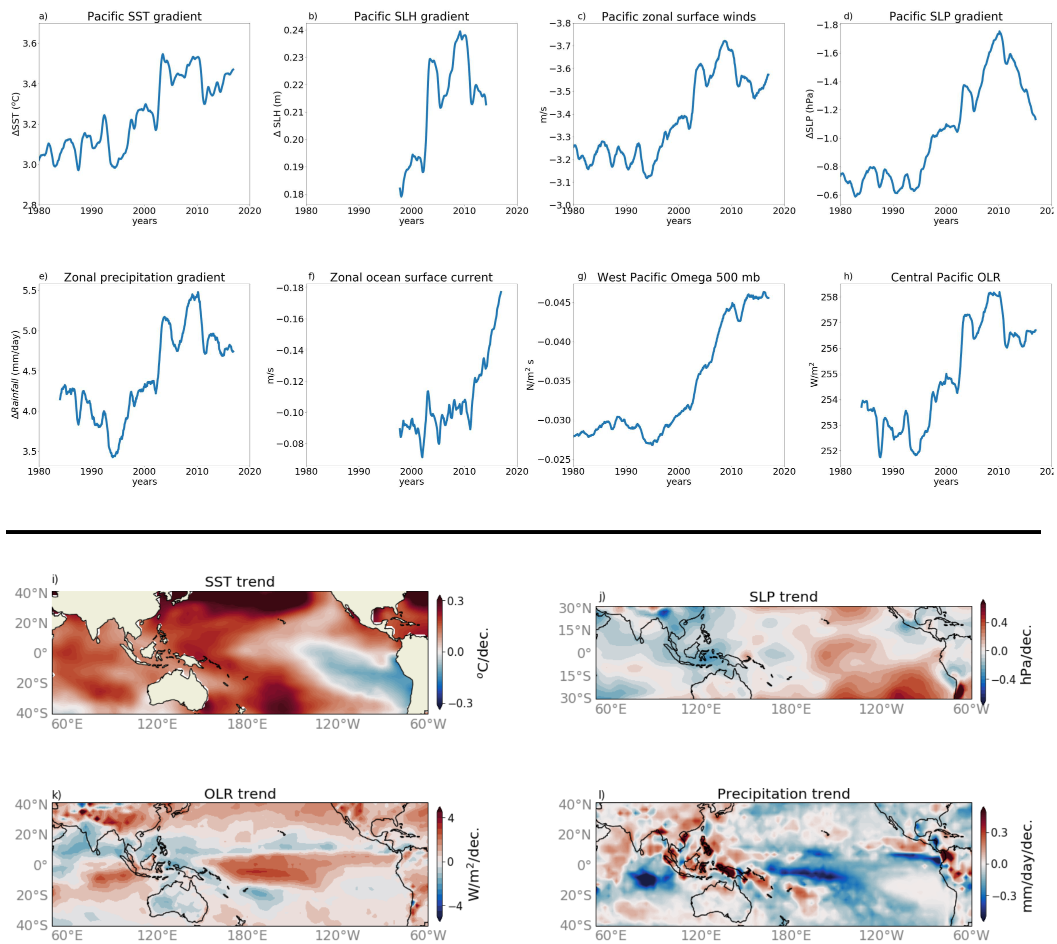

Figure 1. Temporal and spatial changes in the Pacific Walker circulation since the 1980s reflected in different atmospheric and oceanic variables. *The climate indices and datasets used for a-h) are described in detail in the Methods and summarized in Supplementary Table 1. A 10-year running mean is applied. The maps of i-l) show the spatial structure of changes associated with the strengthening of the Walker circulation in the tropical Pacific. Note the cooling of the eastern equatorial Pacific and of the broad region off the coast of South America, resulting in a significant increase in the east-west SST and SLP gradients along the equator.*

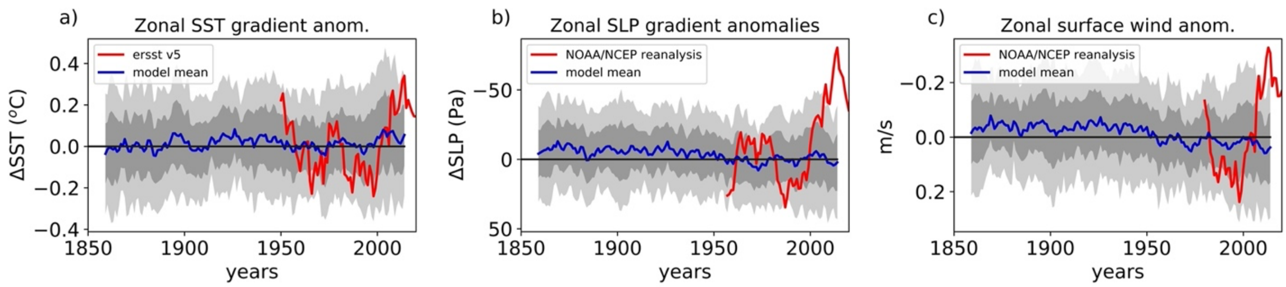

Figure 2. Observed and simulated historical variations in the east-west SST gradient, sea level pressure gradient and zonal surface winds anomalies along the equator *(Methods). Observations are in red; multi-model mean of CMIP6 models is in blue. The model spread across the 40 CMIP6 models is indicated by dark and light grey shadings (one and two standard deviations, respectively). A 10-year running mean is applied before calculating the spread. The observed anomalies of the past decades stay within models' two standard deviations for the zonal SST gradient but exceed two standard deviations for the SLP gradient and zonal winds (note the reverse axis for 3b and 3c). A baseline value is computed and subtracted for each model and the observations to obtain anomalies relative to this baseline. The baseline is calculated from 1950 to 1970 for SST and PSL gradients and 1980 to 1985 for zonal surface wind anomalies due to the unreliability of data prior to this time period.*

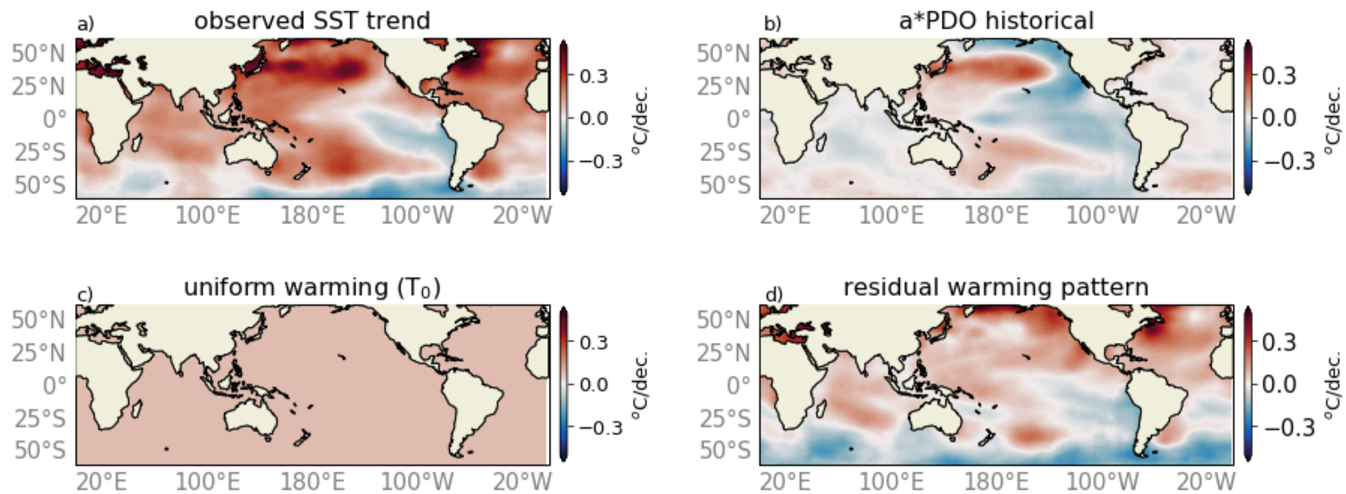

Figure 3. Decomposing the observed SST trends into different components. *(a) The global pattern of the observed local SST trends for years 1980-2020. This pattern is partitioned into three components: (b) a weighted negative PDO pattern; (c) spatially uniform warming trend T_0; and (d) the residual trend pattern once the PDO signal and uniform warming have been subtracted from the full SST pattern. We refer to the residual, in the global context, as the Northern Hemisphere - Indian West Pacific (NH-IWP) warming pattern. The computation of historical PDO is described in Methods. The weight coefficient 'a' is obtained by a least-squares fit between the PDO pattern and the full trend map minus uniform warming.*

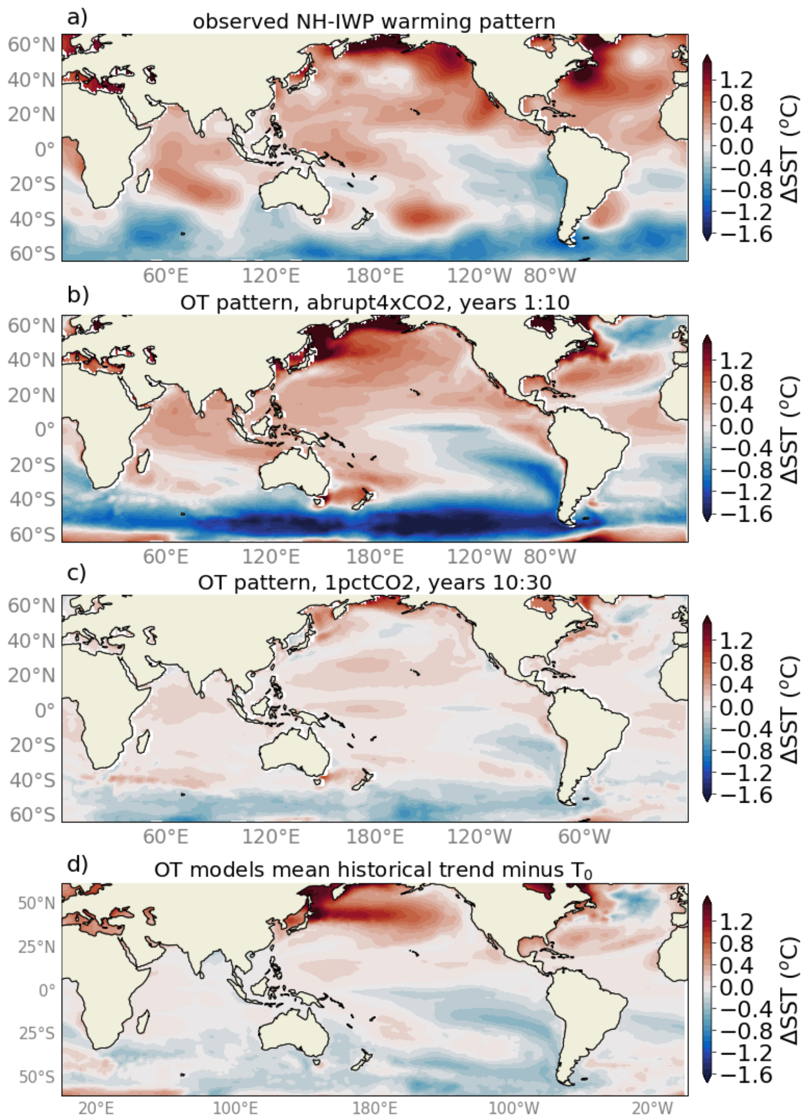

Figure 4. Comparison between the observed NH-IWP warming pattern and OT model SST anomalies for 3 types of experiments. *(a) the observed NH-IWP SST pattern trend (i.e. the residual in Fig. 3d) multiplied by four decades. (b) SST anomalies for the first 10 years of the abrupt-4xCO_2 experiment averaged across OT models (a subset of CMIP6 models with a strong ocean thermostat, see Methods). (c) SST anomalies for the years 10 to 30 in the 1pctCO_2 experiment averaged across OT models. (d) Historical trends for the OT models for years 1980-2015 multiplied by 3.5 decades. Mean warming is subtracted from panels (b),(c) and (d).*